Sixth International Symposium on Turbulence and Shear Flow Phenomena
Seoul, Korea, 22-24 June 2009

DIRECT NUMERICAL SIMULATION OF UNSHEARED TURBULENCE DIFFUSING TOWARDS A FREE-SLIP OR NO-SLIP SURFACE

Julien Bodart, Jean-Bernard Cazalbou, Laurent Joly
Université de Toulouse, Institut Supérieur de l'Aéronautique et de l'Espace (ISAE)
BP 54032 - 31055 TOULOUSE Cedex 4,France
[Julien.Bodart,Jean-Bernard.Cazalbou,Laurent.Joly]@isae.fr

ABSTRACT

The physics involved in the interaction between statistically steady, unsheared turbulence and a blocking surface is highly dependent on the precise nature of the surface, i. e. whether it is a free-slip surface or a solid wall. In this paper, we use direct numerical simulation to investigate the differences between these two situations, the original flow configuration introduced by Campagne et al. (2006a,2006b) has been used as a basis for this comparative study. Two simulations have been performed with strictly identical numerical and physical parameters except for the dynamic boundary condition at the plane surface which is either free-slip (free surface) or no-slip (solid wall). We show that the extent of the blocking effect (outer layer) is strictly the same in both cases. The precise nature of the dynamic boundary condition only influences the inner layers. Both flow configurations have been fully documented including the Reynolds-stress budgets. The differences in the intercomponent energy transfer (pressure-strain correlations) are thoroughly investigated. It is shown that the transfer, although slightly larger in the solid wall case, is a significant contributor to both budgets: the slight difference may be attributed to viscous effects as suggested by Perot and Moin (1995). This is obviously not the case for the net level of the correlation. We suggest that this level – representative of the splat/antisplat imbalance in the Perot-Moin phenomenology – is a consequence of the dissymmetry in the interacting turbulent field.

INTRODUCTION

An original numerical configuration has been designed by Campagne et al. (2006a,2006b) in order to study the interaction between statistically steady, unsheared turbulence and a blocking surface within a direct numerical simulation (DNS) framework. A random force sustains turbulence in a fixed-width plane layer, in the middle of and parallel to two surfaces where the desired boundary conditions are applied (see Fig. 1). After a transient, a statistically steady state is obtained in which turbulence decreases across a pure-diffusion region, before interacting with the surface. In the work of Campagne et al., this configuration was studied using a fully pseudo-spectral Fourier solver. Due to inherent Fourier-solver limitations, the study had to be limited to the case of a free-slip surface boundary condition.

In order to overcome such a limitation, a new solver has been built using a mixed spectral/finite-difference discretization. The free surface and solid wall cases (hereinafter referred to as FS and SW) have been computed with strictly identical forcing fields, fluid properties (density, viscosity), and domain dimensions; thus ensuring a meaningful comparison. Our purpose is twofold: first, to fully document both flow configurations and second, to better understand the physics involved in the intercomponent energy transfer

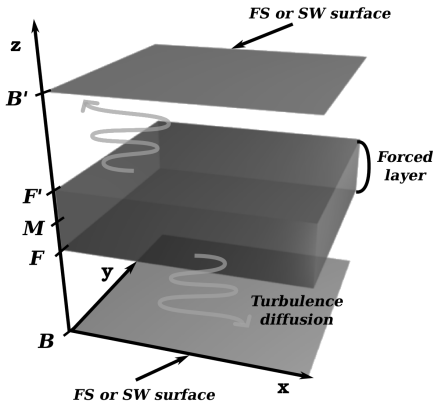

Figure 1: Numerical setup.

mechanism near a blocking surface. As the second point is considered, it is now well established that, while the pressure-strain correlation behaves usually as a return-to-isotropy mechanism, the picture changes drastically in the vicinity of the surface where it promotes energy transfer from the normal to the tangential directions. This is observed in free-surface flows as well as in wall-bounded flows. Such behavior has long been attributed to the "splat effect": due to kinematic blocking, packets of fluid impacting the surface transfer their normal kinetic energy to directions parallel to the surface. This interpretation has later been extended by Perot and Moin (1995) (hereinafter referred to as PM95) to take into account the necessary counterpart of the splat mechanism: the "antisplat" mechanism in which collisions between packets of fluid traveling along the surface may produce ejection of fluid normal to the surface. The splat/antisplat mechanism lead to opposite contributions to the pressure-strain correlation and, consistently, Perot and Moin have suggested that the net level of the correlation should be determined by the imbalance between the two kinds of events. In their comparative study of initially isotropic turbulence decaying in the presence of either a free surface or a solid wall, they further concluded that the action of viscosity was responsible for the imbalance. In our configuration, the Reynolds-stress budgets are not dominated by viscous dissipation and the time variation terms. Instead turbulence is continuously injected into the surface layer by turbulence diffusion from the forcing region. We are thus getting closer to the turbulent boundary layer arrangement with a turbulence production remote from the wall, than previous DNS in which a surface is inserted within a decaying turbulent field. In this paper we point out that these characteristics will help to get a better insight into the physical processes that set the level of the pressure-strain correlation in wall-bounded turbulence.

Numerical setup

The incompressible Navier Stokes equations are solved in a hybrid Fourier/physical space. A pseudo-spectral Fourier algorithm is applied in the two periodic directions, while a sixth-order compact scheme (Lele, 1992) is preferred along the surface-normal direction. A new random forcing has been defined and implemented (Bodart et al., 2008) within the mixed Spectral/Physical space. The major difficulty was to localize this forcing in space while satisfying the following constraints: the forcing must be active at large scales only, divergence-free and decorelated in time.

Presentation of DNS cases

The number of grid points is the same in both cases: 224x224 dealiased modes in the x and y direction, 288 points in z, the wall-normal direction. The same cosine type stretching is used in the z direction in both cases and ensures a statistically equivalent behavior in the forced layer. The resulting Reynolds numbers based on the turbulent length scale $l = k^{3/2}/\epsilon$ and on the Taylor micro length scale are shown in table 1.

		Free-slip surface		*No-slip wall*	
Location	$z/\mathcal{L}$	Re_{λ_f}	Re_l	Re_{λ_f}	Re_l
M	12.8	145	1225	142	1225
F	8.5	66	150	66	150
B	0.	44	114	0	0

Table 1: Characteristic Reynolds numbers, at three z-locations, M: middle plane F: forced layer edge B: Boundary plane.

Statistics generation

In this configuration, the time scale grows across the diffusive layer, and reaches a maximum at the surface in the FS case and slightly above the wall the in the SW case. Based on the value $T^* = \max[\overline{k}/\overline{\varepsilon}(z)]$, statistics were gathered during 10 time units in both the SW and FS cases. Total computations required around 12000 CPU hours on the IBM/POWER6 platform at IDRIS(Paris).

FLOW STRUCTURE

The flow structure involves several distinct regions as, starting from the forced layer, turbulence diffuses toward the surface until the presence of the latter is felt.

The pure-diffusion region.

In this region, the flow structure is governed by a balance between turbulent diffusion and dissipation. In oscillating-grid experiments (see for instance De Silva and Fernando, 1994), the lengthscale linearly increases with the distance to the turbulent source while the turbulent kinetic energy decreases.

The velocity and vorticity isotropy factors, defined respectively as $I_u = w'/u'$ and $I_\omega = \omega'_x/\omega'_z$ are plotted in Fig. 2. I_u reaches a value of 1.14 in the region where the length scale is linear. This is in agreement with the constant value given by De Silva and Fernando (1.18).

The outer blockage layer.

Further away from the forced layer and closer to the surface, the flow enters a surface-influenced layer, which is subject to (i) the kinematic (impermeability) condition, and (ii) the dynamic (free-slip or no-slip) boundary condition. The influence of the kinematic condition is felt farther from the surface than that of the dynamic boundary condition; for this reason the surface-influenced layer can be denoted as the outer "blockage" layer. The latter includes, adjacent to the surface, an inner "slip" or "viscous" layer (depending on the precise nature of the dynamic boundary condition).

The influence of the impermeability condition (according to which the surface-normal velocity component cancels at the surface) can be traced through the behavior of the velocity isotropy factor. The blockage layer can be defined as the region across which it goes from its pure-diffusion value (1.14 here) down to zero at the surface. Figure 2 shows this evolution, the most striking feature is the very similar behavior in both cases, despite very different turbulent energy levels close to the surface (one order of magnitude smaller in the SW case than in the FS case when the surface asymptotic behaviors are considered). A major conclusion that arises is that the normal extent of the blocking effect *does not depend* on the precise nature of the dynamic boundary condition.

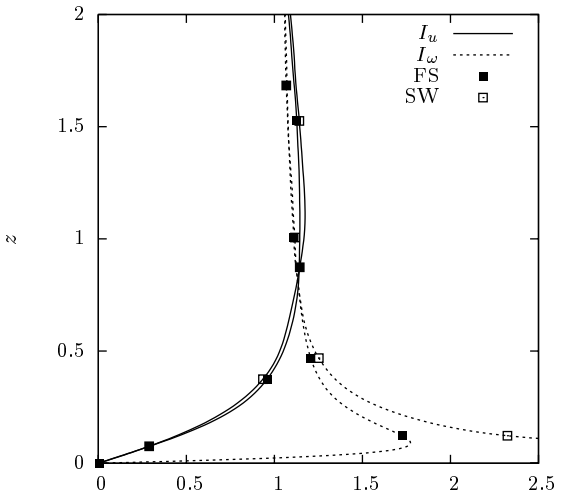

Figure 2: Isotropy factors I_u and I_ω (the vertical coordinate is not normalized).

We also substantiate the point, introduced in Campagne et al. (2006a), according to which the length scale $\mathcal{L} = \left(dI_u/dz|_{z=0}\right)^{-1}$ can be used as a measure of the blockage layer thickness. Very close values are found in the two cases: 0.234 and 0.236 respectively in the FS and SW case. The actual thickness of the the outer blockage layer is about $4\mathcal{L}$ (Campagne, 2006b). The $\mathcal{L}$ quantity will be used in the following to normalize the vertical coordinate.

The inner layers

An essential difference between the two boundary conditions arises from their consequences on the vortex dynamics near the surface: the free-slip condition yields a vorticity vector normal to the surface while the no-slip condition imposes that it becomes tangential. Figure 2 shows the evolution of the vorticity isotropy factor I_ω. It stresses the difference between the two cases : (i) in either FS and SW cases, I_ω increases towards the surface in the upper part of the outer layer – this is a blockage layer effect; (ii) closer to the wall,

I_ω goes to zero in the FS case while it goes to infinity in the SW case. In the FS case, the thickness of the inner slip layer can be defined as the distance to the surface at which I_ω reaches its maximum, while in the SW case, the inner viscous layer could be defined according to the kinetic energy profile (not shown here).

REYNOLDS STRESSES BUDGETS

In this configuration the flow is statistically axisymmetric and the Reynolds-stresses budgets reduce to:

$$\begin{aligned} 0 &= -\frac{\partial \overline{u^2 w}}{\partial z} + \nu \frac{\partial^2 \overline{u^2}}{\partial z^2} + 2\overline{\frac{p}{\rho}\frac{\partial u}{\partial x}} - 2\nu \overline{\frac{\partial u}{\partial x_k}\frac{\partial u}{\partial x_k}} \\ &= \mathcal{D}^u_{11} + \mathcal{D}^\nu_{11} + \Pi_{11} - \varepsilon_{11} \qquad (1) \\ 0 &= -\frac{\partial \overline{w^3}}{\partial z} + \nu \frac{\partial^2 \overline{w^2}}{\partial z^2} + -2\overline{\frac{\partial p w}{\partial \rho}} + 2\overline{\frac{p}{\rho}\frac{\partial w}{\partial z}} - 2\nu \overline{\frac{\partial w}{\partial x_k}\frac{\partial w}{\partial x_k}} \\ &= \mathcal{D}^u_{33} + \mathcal{D}^\nu_{33} + \mathcal{D}^p_{33} + \Pi_{33} - \varepsilon_{33} \qquad (2) \end{aligned}$$

Thus $\mathcal{D}^u$ and $\mathcal{D}^p$ on the one hand, and $\mathcal{D}^\nu$ on the other, respectively denote turbulent and viscous diffusion while $\epsilon_{\alpha\alpha}$ stands for the dissipation of $\overline{u_\alpha u_\alpha}$. Figures 3 and 4 respectively display the surface-normal evolution of the tangential and normal kinetic energy budgets.

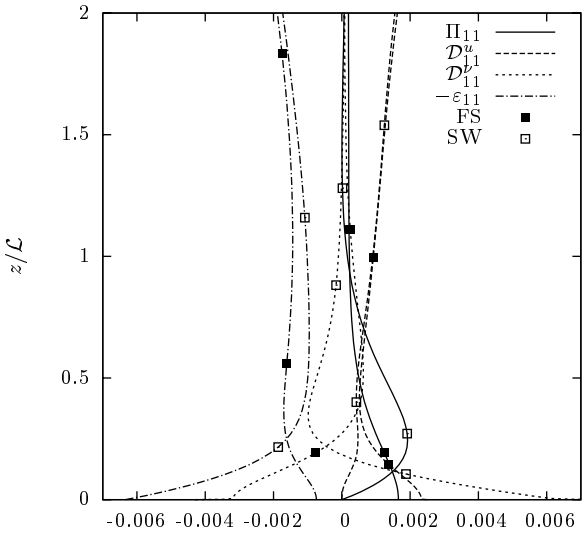

Figure 3: Surface-normal profile of the tangential Reynolds Stress budget.[1]

In the FS case, the budgets are remarkably consistent with those by obtained by Campagne et al. (2006a). Outside the inner layer, the magnitudes of the different terms are very similar to those found in the SW case. However, we get a clear contrast in the inner layer in response to the slip versus no-slip condition at the surface: viscous diffusion balances dissipation in the no-slip case while both of them act in the same way and balance the turbulent diffusion in the SW case. The pressure-strain correlation plays a similar role in both cases. In the near-surface region it is a sink term for the normal stress and a source term for the tangential stress. This expected feature was already described by Walker et al. (1996) and PM95. In contrast with the standard return-to-isotropy effect embedded in the pressure-strain correlation remote from the wall, the intercomponent

[1]We plot here raw values in order to make proper comparisons. Nevertheless the value of the dissipation $\varepsilon = 1/2 \cdot \varepsilon_{ii}$ at the surface reach $\varepsilon_s = 0.00648$ and $\varepsilon_s = 0.001275$ in the no-slip and free-slip case respectively.

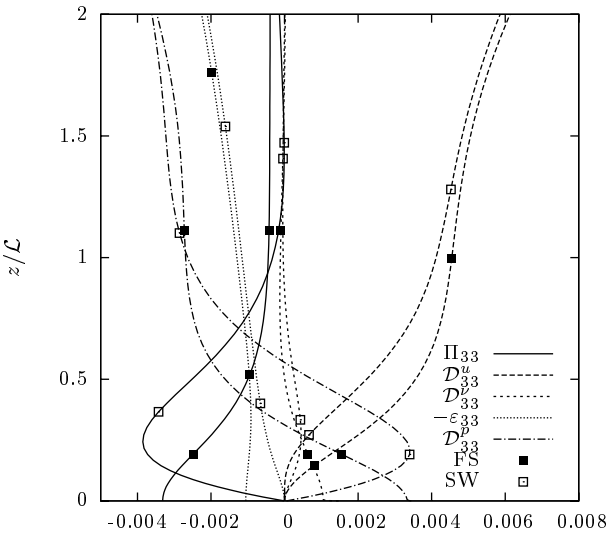

Figure 4: Surface-normal profile of the normal Reynolds Stress budget.[1]

energy transfer is thus reversed and produces anisotropy in the near-surface region. The interpretation given by PM95 relies upon the splat and antisplat mechanisms according to which energy is removed from the normal component and transferred the tangential one (splat) and conversely from the tangential component to the normal one (antisplat). It was further claimed that viscous friction along the wall prevents that all kinetic energy, transferred to the tangential component by the splat event, be restored to the normal component by the antisplat event. In our simulations, it appears that viscous friction only accounts for a minor increase in the magnitude of Π_{33} in the SW case as compared to the FS case. Interestingly, the pressure-strain keeps the same order of magnitude in both cases. This suggests that another reason has to be found to explain the splat/antisplat imbalance.

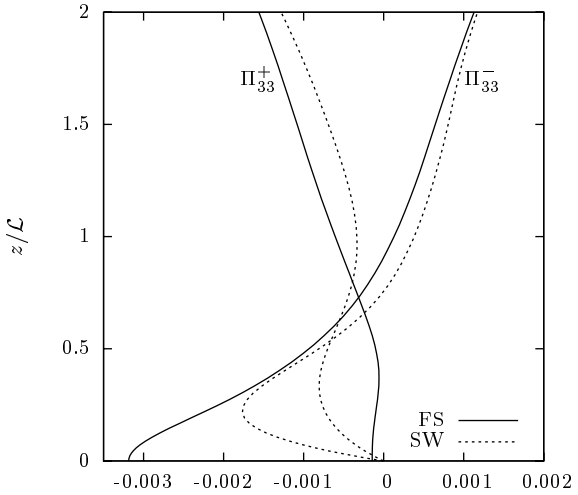

Figure 5: Normal pressure strain correlation decomposition[1] using the sign of $\partial w/\partial z$.

INTERCOMPONENT ENERGY TRANSFER

The splat/antisplat phenomenon being related to impact/ejection of fluid along the normal direction, it can be traced in instantaneous fields by following the sign of the normal velocity component. Moreover, due to the vanishing of the normal velocity at the surface in both cases, its normal derivative, $\partial w/\partial z$, and w itself exhibit similar distributions in the close neighborhood of the surface. Splat events, associated with fluid packets moving towards the surface, are thus characterized by negative $\partial w/\partial z$. Antisplat events, or fluid packets moving away from the surface yield positive values of the vertical strain $\partial w/\partial z$. Accordingly, we split the contributions to the normal pressure-strain correlation Π_{33} in two parts, Π_{33}^{+} and Π_{33}^{-}, by applying a conditional sampling based on the sign of $\partial w/\partial z$.

Figure 5 shows such a decomposition in the SW and FS cases. In both situations, the sign of the Π^{-} correlation switches to negative in the vicinity of the boundary, in agreement with the concept of splats driving normal kinetic energy from the normal to the tangential components. The Π^{+} correlation, almost vanishes at the free-slip wall and unexpectedly brings an extra negative contribution to Π_{33}^{-} in the no-slip case. We thus suggest that the intercomponent transfer represented by Π_{33} results from a more complex mechanism than a simple disequilibrium between splats and antisplats as advocated by PM95. We will now take a closer look to these elementary events and try to decipher the way they contribute to the pressure-strain correlation.

Quadrant decomposition

In order to understand how local events can build up the pressure-strain correlation, we unfold its content in the $(p, \partial w/\partial z)$ plane at a given distance from the surface, say z_0. To reach statistical convergence, we collect data from 35 instantaneous fields every $\Delta t/T^* = 0.15$, thus basing our analysis on close to four million samples for each displayed dataset. Figures 6 and 7 show isocontours of the contribution to Π_{33} at $z_0 = 0$ in the FS case and at $z_0 = 0.25\mathcal{L}$ in the SW case. These values have been selected in order to ensure that the pressure-strain correlation is of the same order of magnitude in both cases. A logarithmic scale is used to maximize the number of visible events.

Figure 6 refers to the FS case. It shows that most of the samples are found when the pressure fluctuation and the vertical strain are close to their *rms* values. We also observe a small number of realizations located far from the origin in the lower-right quadrant. These events exhibit the expected features of splats since positive pressure fluctuations, $p > 0$, result from fluid packets impacting the surface, $w < 0$ or $\partial w/\partial z < 0$. Tables in Fig. 6 give the cumulative contribution to Π_{33} and the integrated joint probability function from each quadrant. With 1.83 times Π_{33} coming from splat events, representing only 19.5% of the samples, we conclude that the energy transfer is driven at first order by a small number of high-intensity splat events. Standard antisplat events are located in the upper-right quadrant, i.e. associated to a local pressure rise as fluid packets traveling along the surface impact each others. They are represented by scarce incursions towards large fluctuations of pressure and strain. However, they are seen to be as likely and contribute in the same proportion to Π_{33} as those lying in the two last quadrants (lower-left and upper-left). The content of which cannot be clearly associated with a definite pressure response to a local kinematic pattern.

In figure 7, referring to the SW case, we notice two majors differences with the FS case. The first one is the complete disappearance of the antisplats, together with a significant reduction in the strain-rate intensity in the upper-right quadrant. This can probably be attributed to the

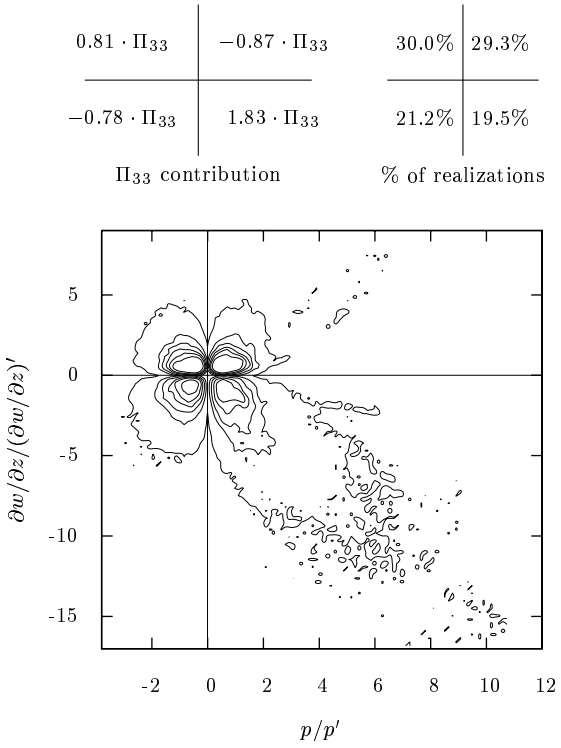

Figure 6: Contribution in the Π_{33} correlation, for the FS case, at $z/\mathcal{L} = 0$. Both axis are normalized using their respective rms values.

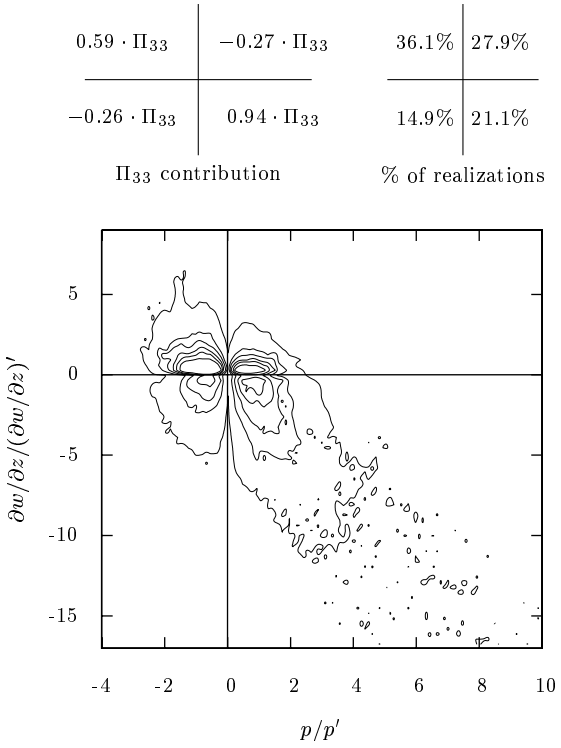

Figure 7: Contribution in the Π_{33} correlation, for the NS case, at $z/\mathcal{L} = 0.25$. Both axis are normalized using their respective rms values.

viscous effects, which slow down the fluid particles moving along the wall before producing an antisplat, thus verifying the conjecture of PM95. The second one is the net disequilibrium between the two upper quadrants, which leads to a negative global contribution to the pressure-strain correlation. This is in agreement with Fig. 5 but cannot be clearly explained at this stage.

We can now consider that the splat and antisplat processes refer to a small number of *correlated* events. They derive from high intensity normal strain rates, able to dominate the non-local contributions in the resulting pressure field. This local correlation is responsible for opposite directions in the intercomponent energy transfer. Figure 8 shows the correlation coefficient which compares the pressure-strain correlation and the *rms* value of each term involved. Its low value far from the surface shows that the pressure fluctuation and the strain rate are almost uncorrelated, while its increase close to the SW/FS region suggests the occurence of correlated events.

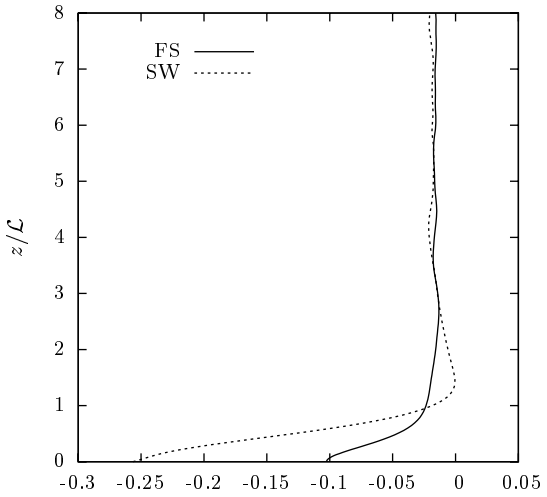

Figure 8: Correlation coefficient for the normal pressure strain term Π_{33}: $c(z) = |\Pi_{33}|/[p' \cdot (\partial w/\partial z)']$.

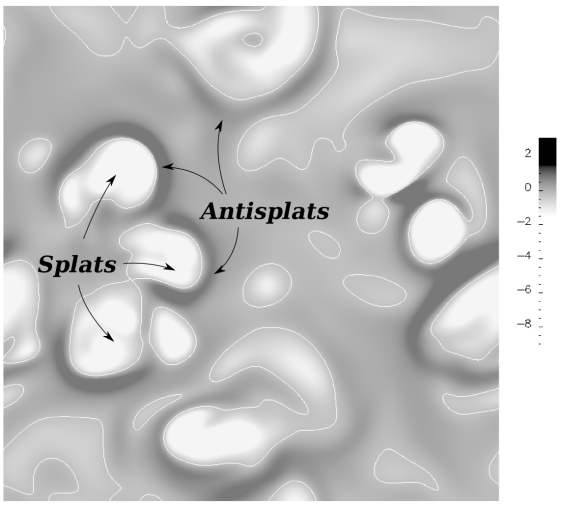

Figure 9: Map of the $\partial w/\partial z$ field at $z/\mathcal{L} = 0$, in the FS case. Normalization is coherent with Fig. 6.

Figures 9 and 10 illustrate the aforementioned characteristics of the splat/antisplat events, using the field $\partial w/\partial z$ to separate regions of motion toward or from the surface. Nearly circular impacts of fluid moving toward the free surface look like the interaction of a jet with a surface. The most striking feature in the FS case is the presence of antisplats surrounding the splats. It is worthwhile to notice the very high intensity of the splats as compared to that of the antisplats. In order to satisfy the continuity equation, large areas of fluid slowly leaving the surface compensate for the presence of few localized splats.

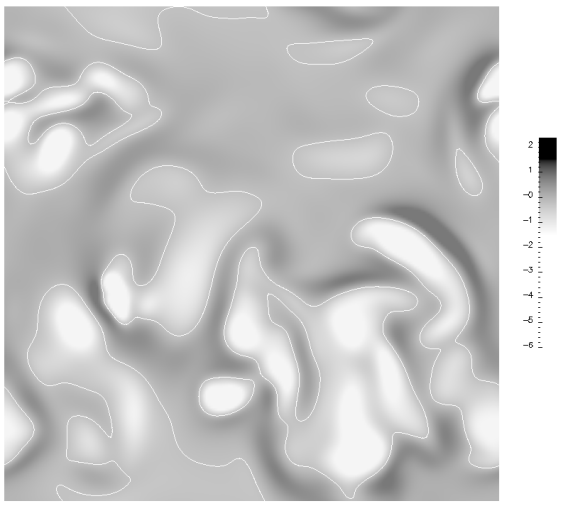

Figure 10: Map of the $\partial w/\partial z$ field at $z/\mathcal{L} = 0.25$, in the SW case. Normalization is coherent with Fig. 7.

Splat/anti-splat imbalance.

In their numerical experiment, where the boundary condition is suddenly imposed at the edge of a cubic domain filled with decaying homogeneous turbulence, PM95 noticed that the order of magnitude of this energy transfer was relatively low in the FS case as compared to that observed in the SW case. They suggest that the disequilibrium between splat/antisplat in the latter case is controlled by the viscosity which slows down the fluid packets moving along the wall before being ejected back into the flow; while in the FS case, the absence of friction at the surface leads to a global equilibrium. In a similar simulation but at longer time, Walker et al. (1996) introduced the idea that the return-to-isotropy mechanism was still present in the near surface region. It should act against the splat phenomenon, and therefore leave a significant amount of energy transfer at short time (low anisotropy level), and conversely inhibit the transfer at longer time (high anisotropy level). In our experiment, (i) the isotropy level is identical in both cases (see Fig. 2), and therefore the amount of energy transfer through the return-to-isotropy mechanism should be the same, (ii) the magnitude of the pressure-strain correlation is comparable in both cases, which suggests another reason than viscosity for the imbalance between splats and antisplats (iii) the imbalance appears as slightly higher in the SW case which does not rule out that viscosity still plays some role.

In order to find the reason for the imbalance between the two kinds of event, we will try to evaluate the consequences of the dyssymmetry observed above in the velocity gradient distribution: small/large areas of fast/slow fluid moving toward/from the surface. The tables in Fig. 6 help to quantify this dissymmetry: when adding the percentage of realizations of events with a positive/negative normal strain rate,

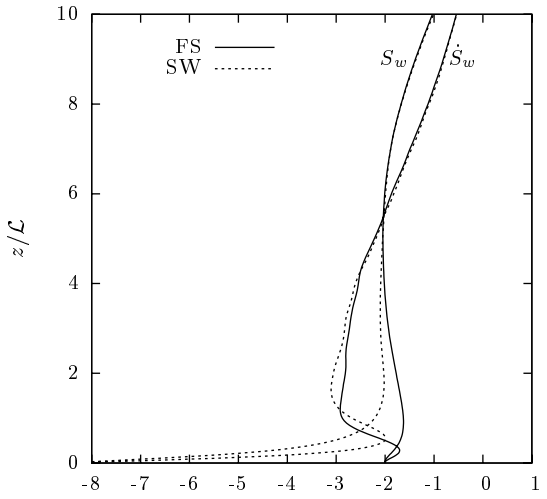

Figure 11: Normal-velocity skewness S_w and normal-velocity-gradient skewness $\dot{S}_w$.

it leads to a large imbalance of 60% against 40%, in favor of the ejection events. The SW cases reveals an even higher imbalance (64%-36%). In terms of probability density function, it is consistent with a negative skewness. In Fig. 11, we present the skewness of normal-velocity S_w and that of the normal-velocity derivative $\dot{S}_w$, which represent the dissymmetry in the normal-velocity and normal-velocity-gradient fluctuating fields. Some basic physical considerations are necessary to understand how such a dissymmetry can lead to a significant imbalance between splat and antisplat events. Indeed, any linear process would result in a perfect equilibrium with or without dissymmetry. However if we consider the stagnation points created by both events, the overpressure Δp should be of the order of ρw^2. Due to this quadratic relation between pressure and normal velocity, the few number of high intensity impacts will correlate with significantly higher pressure fluctuations, as compared to those associated to the large number of dull ejections. Thus, even if the continuity equation requires that fluid moving from the surface be balanced by fluid moving to the surface, the dissymmetry in the normal velocity or strain-rate fields can produce unexpected inter-component energy transfers. From the skewness profiles, we can infer that the disequilibrium between splat and antisplat is created *away* from the surface. By slower motions coming from the wall, the dissymmetry and therefore the skewness are enhanced by viscosity in the SW case. More generally, the origin of the disequilibrium comes, in the first place, from the intrinsic nature of the turbulence interacting with the surface and, in the second place, should be affected by the viscosity in the case of a SW condition. As compared to the case of decaying homogeneous turbulence studied by PM95, the pure-diffusion flow configuration investigated here reinforce this mechanism by producing a non-zero skewness in the velocity distribution (see also the experiments by Risso and Fabre, 1997, in which velocity skewness close to -1 were reported).

CONCLUSION

In the study of the interaction between sustained turbulence diffusing from a plane source and either a free-surface or a solid wall, several important conclusions seem to be reached. First, it appears that the anisotropy of the velocity field is insensitive to the precise nature of the dynamic boundary condition. In other words, kinematic blocking is felt at the same distance from the surface in the case of a free-surface flow or in the case of the solid wall flow. Second, important information has been obtained on the way the pressure-strain correlation and correspondingly the intercomponent energy transfer build up from elementary events. Referring to the splat/antisplat phenomenology introduced by Perot and Moin, it appears that in both cases, energy transfer flows from the normal component to the tangential components. Its amount is indeed determined by the disequilibrium between splats and antisplats, but this disequilibrium mostly mirrors the dissymmetry of the interacting fluctuating field (measured by the skewness of the velocity or velocity-derivative fluctuating fields). However the quadrant decomposition shown in Fig. 7 seems to indicate that the splat/antisplat balance in the solid-wall case can only account for two thirds of the global amount of intercomponent energy transfer: the remainder corresponds to processes involving negative pressure fluctuations which suggests that rotational events are to be considered in order to fully elucidate the mechanisms involved in this case.

ACKNOWLEDGMENT

Preliminary computations were carried out under the HPC-EUROPA++ project (project number: 1187), with the support of the European Community - Research Infrastructure Action of the FP7 “Coordination and support action” Programme. Final computation were carried out on the IBM/POWER6 supercomputer at IDRIS (Paris).

REFERENCES

Bodart, J. and Joly, L. and Cazalbou, J.-B., 2008, “Local large scale forcing of unsheared turbulence”, In press, *7th Direct and Large Eddy Simulation Conference.*

Campagne, G. and Cazalbou, J.-B. and Joly, L. and Chassaing, P., 2006a, “Direct numerical simulation of the interaction between unsheared turbulence and a free-slip surface”, *In Proceedings of ECCOMAS CFD 2006 Conference.*

Campagne, G. , 2006b, “Simulation numérique directe de l’interaction turbulence/surface libre pour l’analyse du transfert intercomposantes.” Thèse de doctorat, INP Toulouse.

De Silva, I. P. D. and Fernando, H. J. S., 1994, “Oscillating grids as a source of nearly isotropic turbulence”, *Phys. Fluids*, 6(7):2455-2464.

Risso, F. and Fabre, J., 1997, “Diffusive turbulence in a confined jet experiment”, *J. Fluid Mech.*, 337(-1):233-261.

Lele, K. S., “Compact finite difference schemes with spectral-like resolution”, *J. Comp. Phys.*, 103(1):16-42.

Perot, B. and and Moin, P., 1995, “Shear-free turbulent boundary layers. part 1: Physical insights into near wall turbulence”, *J. Fluid Mech.*, 295:199-227.

Walker, D. T., Leighton, R. I., and Rios, G. L. O., 1996. “Shear-free turbulence near a flat free surface”. *J. of Fluid Mech.*, 320(-1):19-51.